JACS
JOURNAL OF THE AMERICAN CHEMICAL SOCIETY
Article
pubs.acs.org/JACS

Fortification of CdSe Quantum Dots with Graphene Oxide. Excited State Interactions and Light Energy Conversion

Ian V. Lightcap and Prashant V. Kamat*

Radiation Laboratory, Department of Chemistry & Biochemistry, University of Notre Dame, Notre Dame, Indiana 46556, United States

Supporting Information

ABSTRACT: Graphene based 2-D carbon nanostructures provide new opportunities to fortify semiconductor based light harvesting assemblies. Electron and energy transfer rates from photoexcited CdSe colloidal quantum dots (QDs) to graphene oxide (GO) and reduced graphene oxide (RGO) were isolated by analysis of excited state deactivation lifetimes as a function of degree of oxidation and charging in (R)GO. Apparent rate constants for energy and electron transfer determined for CdSe−GO composites were 5.5×10^8 and 6.7×10^8 s^{-1}, respectively. Additionally, incorporation of GO in colloidal CdSe QD films deposited on conducting glass electrodes was found to enhance the charge separation and electron conduction through the QD film, thus allowing three-dimensional sensitization. Photoanodes assembled from CdSe−graphene composites in quantum dot sensitized solar cells display improved photocurrent response (~150%) over those prepared without GO.

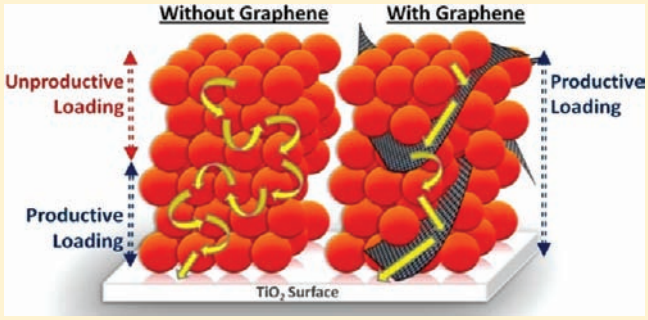

INTRODUCTION

Quantum dot solar cells (QDSCs) have drawn increased interest in recent years due to the ability to tune semiconductor bandgaps, high extinction coefficients, large molecular dipoles, and the potential for multilayer sensitization.[1−4] Most alluring is the potential in QDSCs for multiple electron generation and hot electron utilization, phenomena that boost the theoretical power conversion efficiency beyond the 32% Shockley-Queisser limit in silicon-based solar cells.[5] In spite of these advantages, power conversion efficiencies of ~5% in QDSCs still lag behind their more developed counterpart, the dye-sensitized solar cell. Recent optimization efforts have focused on working electrode surface modifications (e.g., treatment with dipole molecules and ZnS overcoating) and the use of Cu_2S-based counter electrodes.[6−10]

Performance in QDSCs is stunted by limitations in sensitizer loading arising from losses inherent to the nature of electron transport throughout QD networks. Electron conductance within QD films proceeds via electron hopping between orbitals on adjacent QDs, a process termed random walk.[11,12] To arrive at the current-collecting electrode, photogenerated electrons in QDs farther away from the wide bandgap semiconductor (e.g., TiO_2, ZnO, or SnO_2) must successfully complete a greater number electron transfer hopping events without undergoing recombination or trapped-state termination (Scheme 1). In addition to poor electron transfer in thicker QD films, increased QD-layering inhibits electrolyte access to QDs closest to the TiO_2 surface, hindering QD regeneration.[8] Because of these kinetic limitations, most QDSCs utilize near-monolayer loading of the sensitizing semiconductor through linker-assisted deposition of premade colloidal quantum dots, or by in situ formation of QDs on TiO_2 via chemical bath deposition or successive ionic layer adsorption and reaction (SILAR).[13−15]

Scheme 1. Three Electron Transfer Routes from Photoexcited CdSe QDs to a Current-Collecting Electrode Are Depicted[a]

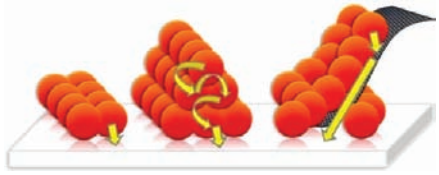

[a]Electron hopping leads to poor film conductivity in thicker QD films (middle QD cluster). The addition of graphene to QD films should promote improved electron transport to the electrode (right cluster).

Graphene composites have been shown in a number of applications to enhance the properties of the host material, particularly in the areas of plastic composites, drug delivery, and energy conversion.[16−23] Enhanced photocurrent and photocatalysis has been previously demonstrated within TiO_2 nanoparticle-graphene composites.[24] Graphene's atomic thinness and large sheet surface area combined with excellent

Received: February 8, 2012
Published: March 29, 2012

   dx.doi.org/10.1021/ja3012929 | J. Am. Chem. Soc. 2012, 134, 7109−7116

electron transport properties make it an ideal material for optimizing electron transport within QD films while minimizing incident light absorption.[25] Preliminary studies of SILAR-synthesized CdSe–graphene, as well as the in situ growth of colloidal quantum dot-graphene composites, have already demonstrated increased photocurrent when compared to nanocrystal-only films.[26,27] While these methods ensure good QD–graphene contact, the effective loading of QD sensitizer is limited to a few monolayers. Careful control of graphene loading is required to extend QD films into the third dimension, where an essential balance must exist between maximizing contact with QDs while minimizing incident light absorption by graphene, which absorbs ~2% of incident light per monolayer.[28] Augmentation of QD loading should enhance QDSC performance, provided that sufficient graphene is present to overcome electron transport limitations resulting from increasing QD film thickness. Incorporating graphene in colloidal QD solutions may prove successful in achieving this aim so long as the graphene maintains a high degree of dispersion during the transition from solution to film.

While nanocrystal–graphene composites have demonstrated enhanced photocurrent and photocatalysis, very little attention has been given to interrogate the excited state interactions between CdSe QDs and graphene. Brus and co-workers concluded that excited state decay from photogenerated electrons in CdSe nanocrystals on pristine graphene decay via Forster resonant energy transfer (FRET).[29] Decay via this pathway does not involve electron transfer and is therefore counterproductive to a semiconductor–graphene composite system designed for improved electron transfer. However, when graphene–QD composites are located within the environment of a photovoltaic device under illumination, the presence of an electrolyte or other hole transporting material serves to regenerate CdSe QDs, enabling continuous charge transfer. Earlier studies from our group have shown the ability of graphene oxide sheets to capture and store electrons from semiconductor nanoparticles.[30] Examination of excited state interactions between QDs and graphene with different levels of oxidation and charging enables us to manipulate energy and electron transfer processes in a controlled fashion. The kinetics of excited state interactions between colloidal CdSe QDs and graphene, and the performance-enhancing qualities of their composites toward the realization of 3-D sensitization in QDSCs are presented.

RESULTS AND DISCUSSION

CdSe–GO and CdSe–RGO Composites. The absorbance spectra of pure CdSe colloidal QDs, pure GO, and RGO dispersions, as well as CdSe–GO and CdSe–RGO composite dispersions, are shown in Figure 1. As expected due to the addition of graphene, a slight increase in absorbance is observed in composite dispersions versus CdSe QDs alone. Also note both the CdSe–RGO composite and RGO dispersions show increased absorbance over CdSe–GO and GO dispersions, respectively. It has been previously shown that reduction of GO results in an increase in absorbance throughout the UV and visible spectrum.[23] This effect is clearly seen by the darker appearance of RGO dispersions (inset Figure 1).

CdSe–GO (and CdSe–RGO) composites were formed by simple mixing with sonication. Transmission electron microscopy (TEM) was used to observe the extent of CdSe QD physisorption to individual graphene sheets. TEM images in Figure 2 show submonolayer loading of CdSe QDs (diameter ~3.8 nm) on typically mono- to few-layered graphene sheets.

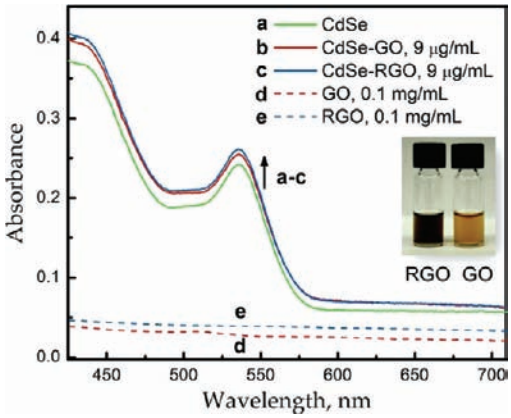

Figure 1. Absorbance profiles of CdSe and CdSe–(R)GO composites. Traces for GO and RGO in ethanol (dotted traces d and e) also included. Solutions (a–c) contain 9% ethanol.

Excited State Interactions. Degree of oxidation within graphene was used to isolate the contribution of the electron transfer pathway during excited state deactivation of CdSe quantum dots by graphene oxide in CdSe–GO composite dispersions. Both GO and RGO are good electron acceptors, however, GO has a higher capacity to consume electrons due to its oxidation state. This allows us to use CdSe fluorescence-quenching as a probe to distinguish the extent of excited state electron transfer to GO and RGO.[31,32] Following initial electron transfer resulting in partial reduction of GO, additional electron transfer leads to storage of electrons.[30] However, continued irradiation makes further transfer of electrons increasingly difficult as a consequence of the GO reduction and subsequent charging. Charge transfer events between photoexcited CdSe and GO are summarized in eqs 1–4. GO reduced by electron transfer from photoexcited CdSe is hereafter referred to as rGO to distinguish it from prereduced RGO.

$$\mathrm{CdSe} + h\nu \rightarrow \mathrm{CdSe(e + h)} \quad (1)$$

$$\mathrm{CdSe(e) + GO \rightarrow CdSe + rGO} \quad (2)$$

$$\mathrm{CdSe(e) + rGO \rightarrow CdSe + rGO(e)} \quad (3)$$

$$\mathrm{CdSe(h) + C_2H_5OH \rightarrow CdSe + {}^{\bullet}C_2H_4OH} \quad (4)$$

Concentration-Dependent Quenching of CdSe Emission. Photoluminescence quenching spectra displayed in Figure 3 reveal that both RGO and GO serve as effective quenchers of excited CdSe. Both reduction and electron storage (reactions 2 and 3) govern the quenching by GO while reaction 3 dominates the quenching by RGO. This difference is reflected in the quenching efficiency. GO quenches more efficiently than RGO at all concentrations, confirming its greater electron-accepting capacity (inset, Figure 3). The highly interactive nature of GO is also evidenced by the strong quenching response which occurs even at the smallest GO concentrations (9 μg/mL), in which nearly 95% of CdSe photoluminescence (PL) is effectively quenched.

The excited state electron transfer and/or energy transfer are responsible for the quenching of CdSe emission. The extent of energy transfer between donor (CdSe) and acceptor species (GO or RGO) is dependent on the proximity and spectral

dx.doi.org/10.1021/ja3012929 | J. Am. Chem. Soc. 2012, 134, 7109–7116

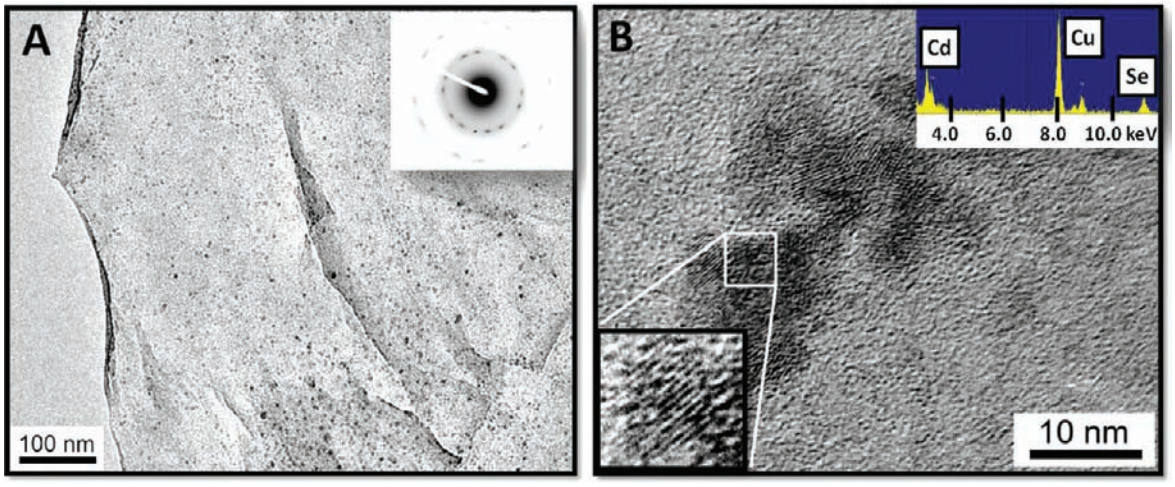

Figure 2. (A) TEM micrograph of GO (on holey carbon grid) after illumination (>420 nm) of CdSe-GO dispersion. Inset shows a selected area diffraction pattern exhibiting the characteristic reciprocal lattice spacings of 1.23 and 2.13 Å. (B) High resolution image of CdSe QDs on graphene. Inset is the energy dispersive X-ray spectrum confirming the presence of CdSe.

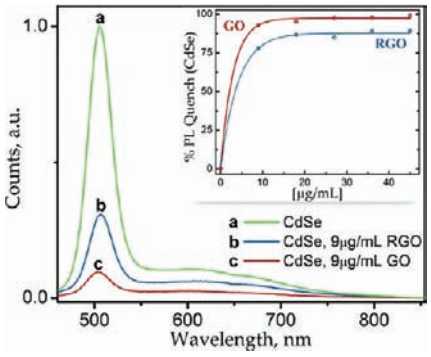

Figure 3. Quenching of CdSe QD photoluminescence by GO and RGO. Inset shows effective quenching even at low graphene concentration (excitation wavelength 373 nm, 420 nm long pass filter).

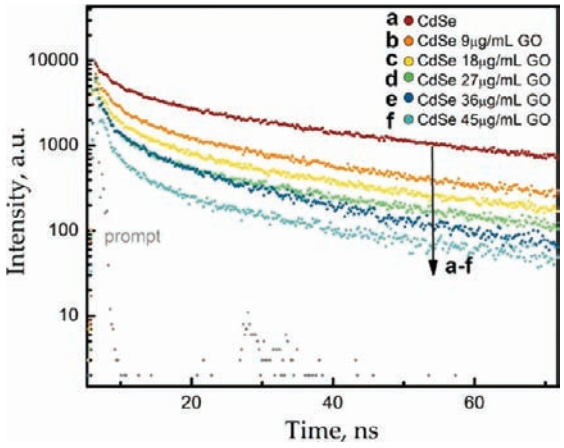

Figure 4. As the GO concentration increases, CdSe photoluminescence lifetimes become successively shorter. Excitation wavelength = 453 nm; long pass filter = 500 nm; fluorescence monitored at 508 nm.

overlap between the two. If the excited state relaxation pathway occurs primarily via energy transfer, then increased optical density of RGO over GO should enable improved overlap with CdSe QD fluorescence, resulting in larger quenching efficiencies with respect to GO. However, GO is instead shown to be the more effective quenching agent. This is most likely the consequence of GO's electron accepting ability combined with its highly interactive nature. The results provide further evidence that, in addition to energy transfer, an electron transfer pathway serves to control the excited state deactivation from CdSe to GO and RGO.

Figure 4 compares CdSe emission decay traces as a function of increasing GO concentration. Consistent with PL quenching results, increasing concentrations of GO successively decrease the PL lifetime of CdSe QDs. Decay traces were fit using a biexponential decay.

With increasing GO concentration, the fast time decay component (τ_1) shows a slight decrease, from 3.24 to 0.93 ns over the range of GO concentrations of 9−45 μg/mL, while its contribution to the overall PL lifetime increases from 78.9% to 94.5% (Table 1). This increased contribution from the fast decay component is attributed to quenching of CdSe PL by GO through energy and electron transfer and suggests considerable interaction between the two (also see ultrafast transient absorption studies in Supporting Information). Using eq 5,

Table 1. Pre-Exponential Fraction from the Double Exponential Fitting Function Shows an Increasing Contribution from the Fast Decay Component (τ_1) to the Overall Decay

GO, μg/mL	τ_1, ns	τ_2, ns	$a_1/(a_1 + a_2)$, %	$a_2/(a_1 + a_2)$, %
0	5.13	44.0	66.1	33.9
9	3.24	35.3	78.9	21.1
18	2.39	32.7	83.9	16.1
27	1.71	29.6	89.1	10.9
36	1.49	26.9	89.4	10.6
45	0.93	23.3	94.5	5.5

we calculate the apparent rate of nonradiative excited state decay, k_{NRD}, to be 8.8×10^9 s^{-1}

$$k_{NRD} = \frac{1}{\tau_{1(CdSe-GO)}} - \frac{1}{\tau_{1(CdSe)}} \quad (5)$$

The lifetime of the slow decay component (τ_2), which mainly arises from the free CdSe quantum dots in the suspension, shows a variance of 44−23.3 ns as we increase the

dx.doi.org/10.1021/ja3012929 | J. Am. Chem. Soc. 2012, 134, 7109−7116

Scheme 2. (Left) Initial Illumination of CdSe−GO Composite Results in Electron Transfer from the CdSe Conduction Band to GO and (Right) Continued Illumination of the System Results in the Reduction of GO and Eventual Storage of Electrons Resulting in a Decrease in Electron Transfer Rate

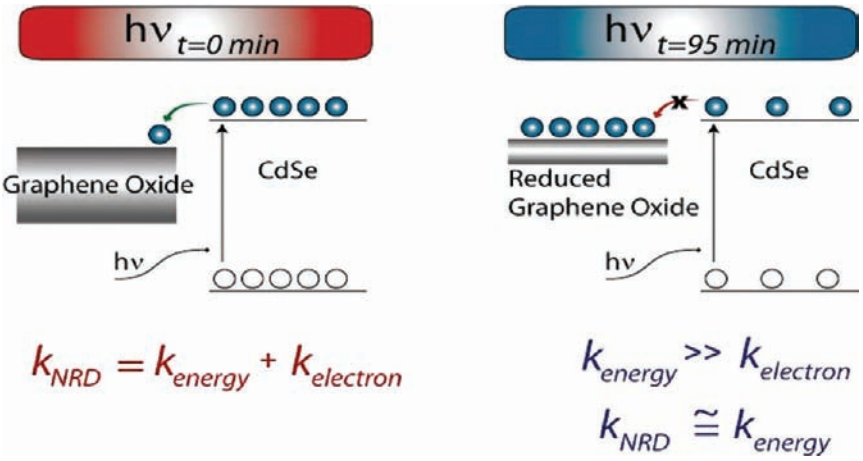

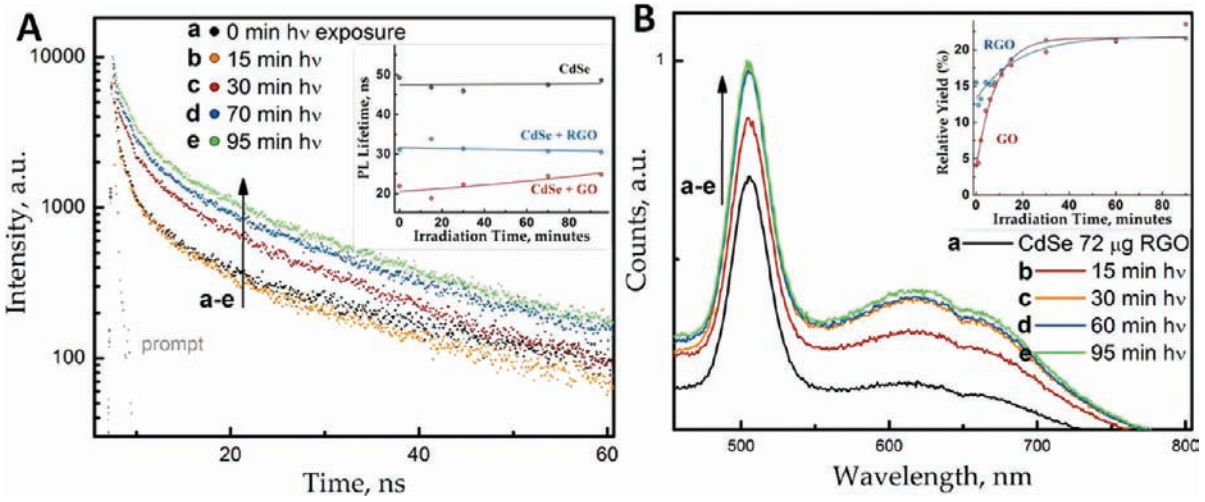

Figure 5. (A) CdSe−GO composites show increased photoluminescence lifetimes upon visible light irradiation (>420 nm). Inset: The effect of visible light illumination (>420 nm) on CdSe photoluminescence lifetimes in the presence of GO and RGO is shown. (B) Emission recovery of CdSe−RGO solution upon illumination with visible light (>420 nm), relative to CdSe only emission. Inset compares the fluorescence recovery of CdSe in GO or RGO.

concentration of GO from 0 to 45 μg/mL. Interestingly, the contribution of the slow component decreases to only about 5.5% at the highest GO concentration. As GO concentrations increase, the number of free CdSe QDs diminish, resulting in a smaller pre-exponential contribution $(a_2/(a_1 + a_2))$ from the long decay component, τ_2. These results confirm the strong interactive nature of GO toward CdSe quantum dots.

Excited State Dynamics Following Prolonged Illumination. It is evident from the emission quenching studies that excited CdSe quite efficiently deactivates on GO/RGO surface. Both electron and energy transfer processes are expected to dominate the deactivation of excited CdSe. The obvious question would then be, how can one isolate these two different quenching mechanisms? As indicated in eqs 2 and 3, electron transfer from photoexcited CdSe QDs to GO results in the formation of rGO, and continued electron transfer to rGO leads to electron storage. The process of GO reduction and electron storage resulting from photoexcited electron transfer from a colloidal semiconductor has been previously described.[23,30] Storage of electrons in rGO should result in diminished electron transfer rates from CdSe QDs to rGO following prolonged illumination. As the electron storage within the graphene network saturates, the electron transfer process slows. Thus, following the prolonged irradiation, it is possible to shut off the electron transfer pathway (right panel in Scheme 2). In the absence of an electron transfer pathway, the emission decay is expected to be dominated solely by the energy transfer pathway.

Emission decay traces of CdSe−GO composites shown in Figure 5A highlight the effect of prolonged illumination on the deactivation of excited CdSe. During early illumination times (0−15 min), the CdSe PL lifetimes remain nearly constant as excited state electron transfer from CdSe results in the reduction of GO. Under these conditions both energy and electron transfer contribute to quenching. At longer illumination times (15−95 min), electron transfer from CdSe QDs to the now-reduced GO (or rGO) results in charging of the graphene network, causing further electron transfer to become increasingly difficult. With the electron transfer pathway unavailable, PL lifetimes necessarily increase as energy transfer

dx.doi.org/10.1021/ja3012929 | J. Am. Chem. Soc. 2012, 134, 7109−7116

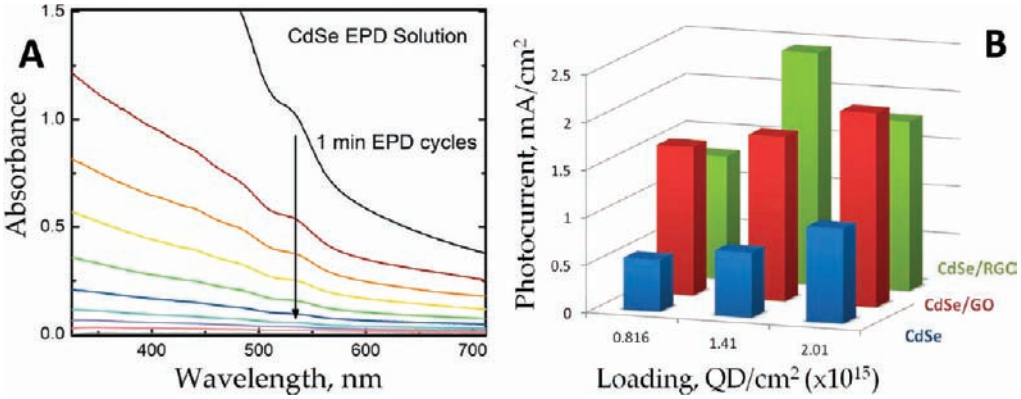

Figure 6. (A) Absorbance of EPD solution by deposition cycle. Solution concentration decreases with each minute, 50 V cycle as CdSe QDs are deposited on electrode. (B) Photocurrent comparison for CdSe and CdSe−(R)GO photoanodes with increased QD loading. Photoanodes were tested in an open cell configuration using 0.1 M Na_2S electrolyte and RGO/Cu_2S counter electrode under 1.5 a.m., 100 mW/cm^2 illumination. Open circuit voltages were ∼0.47 ± 0.03 V with fill factors of 51 ± 3 for all cells tested. GO and RGO concentrations were constant at 20 μg/cm^2.

becomes the only available route for conduction band electrons undergoing nonradiative excited state decay. This effect is confirmed by the increasing PL lifetimes observed in CdSe−rGO composites with prolonged visible light irradiation. As expected, CdSe−RGO composites show similar, but less pronounced, changes in its PL lifetime under similar conditions. The lifetime of CdSe QDs alone during visible irradiation remains unchanged (Figure 5A inset). The effect of visible irradiation on the PL lifetimes of CdSe−(R)GO composites can also be visualized by observation of fluorescence recovery. Both CdSe−GO and CdSe−RGO composites show partial recovery of emission following prolonged visible illumination (Figure 5B), again as a consequence of termination of the electron transfer pathway.

$$(\text{at } h\nu_{t=0\text{min}}) \quad k_{\text{NRD}} = k_{\text{energy}} + k_{\text{electron}} = \frac{1}{\tau_{1(\text{CdSe}-\text{GO},h\nu_{t=0\text{min}})}} - \frac{1}{\tau_{1(\text{CdSe})}} \tag{6}$$

$$(\text{at } h\nu_{t=95\text{min}}) \quad k_{\text{NRD}} \cong k_{\text{energy}} \cong \frac{1}{\tau_{1(\text{CdSe}-\text{GO},h\nu_{t=95\text{min}})}} - \frac{1}{\tau_{1(\text{CdSe})}} \tag{7}$$

$$(\text{at } h\nu_{t=0\text{min}}) \quad k_{\text{electron}} = k_{\text{NRD}} - k_{\text{energy}} \tag{8}$$

$$(\text{at } h\nu_{t=0\text{min}}) \quad k_{\text{electron}} = \left(\frac{1}{\tau_{1(\text{CdSe}-\text{GO},h\nu_{t=0\text{min}})}} - \frac{1}{\tau_{1(\text{CdSe})}}\right) - \left(\frac{1}{\tau_{1(\text{CdSe}-\text{GO},h\nu_{t=95\text{min}})}} - \frac{1}{\tau_{1(\text{CdSe})}}\right) \tag{9}$$

Through comparison of CdSe−GO PL lifetimes before and after illumination, it is possible to estimate the relative rates of electron and energy transfer. Prior to illumination ($h\nu_{t=0\text{min}}$), both electron and energy transfer processes dictate the fast PL lifetime component, τ_1 (eq 6). After extended illumination ($h\nu_{t=95\text{min}}$) and subsequent charging of graphene sheets, the fast component of the excited state relaxation in CdSe QDs proceeds primarily through energy transfer, as electron transfer to charged graphene is shunted. This allows for estimation of the rate of energy transfer in these composites, $k_{\text{energy}} = 5.5 \times 10^8$ s^{-1} (eq 7). Finally, by comparing the difference in the nonradiative decay rates at illumination times t = 0 min and t = 95 min, we estimate the rate of electron transfer in CdSe−GO composites, upon initial illumination, to be 6.7×10^8 s^{-1} (eq 9).

Electrophoretic Deposition of CdSe and CdSe−(R)GO Composites. In order to leverage the benefits of electron transfer observed in CdSe−(R)GO composites, films created from the composites must contain primarily single sheet graphene with a high degree of dispersion. Film deposition of solution-based CdSe−(R)GO composites by means of a drop-cast method typically results in a loss of dispersion between the two species, as well as film inhomogeneity. It is essential for films to achieve a balance between the sufficient supply of graphene for ample QD interfacial contact while also limiting graphene's detrimental filtering of incident light.

The use of electrophoretic deposition (EPD) in composite film preparation has been previously shown to produce films with a good degree of composite homogeneity between CdSe QDs and C_{60}.[33] EPD was employed in the present work to create high quality films of CdSe−(R)GO. The deposition of CdSe QDs was monitored by UV−vis absorbance spectroscopy. Absorption spectra of the EPD solution were taken following each cycle and show successively decreasing dispersion concentrations until deposition of CdSe onto the photoanode is complete (Figure 6A). The difference in QD concentration of the EPD suspension after each cycle corresponds to the amount of QDs deposited on the TiO_2 film. These electrodes were then employed as photoanodes in photoelectrochemical cells consisting of Cu_2S/RGO films as counter electrodes[34] and S^{2-}/S_n^{2-} as the redox electrolyte (Scheme 3).

Photocurrent generated following visible excitation of CdSe/(R)GO films at different loadings of QDs and RGO are shown in Figure 6B. CdSe−(R)GO photoanodes show significant enhancement in photocurrent response over CdSe-only films. The maximum photocurrent was seen at a loading of ∼1.4 × 10^{15} QDs/cm^2 and ∼20 μg/cm^2 RGO. Additionally, the incident photon to current efficiencies (IPCE) of CdSe−(R)GO films were examined to assess the photocurrent response and the role of RGO in improving the efficiency of photocurrent generation. IPCE measurements show that the

dx.doi.org/10.1021/ja3012929 | J. Am. Chem. Soc. 2012, 134, 7109−7116

Scheme 3. Open Cell Configuration in Which Photocurrent Generation Occurs When CdSe QDs Absorb Visible Light, Generating Electron-Hole Pairs[a]

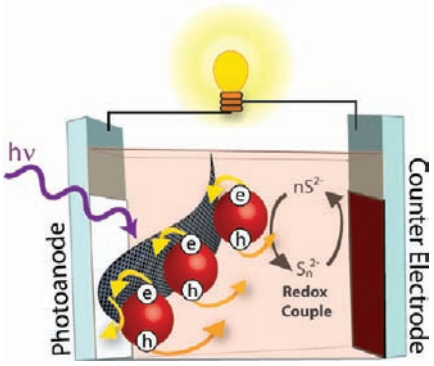

[a]Electrons are injected into RGO and shuttled to the electrode while holes are used to oxidize sulfide to polysulfide. Electrons travel through an external circuit to the RGO/Cu_2S counter electrode, where they reduce polysulfide to sulfide, completing the redox cycle.

presence of RGO in the CdSe enhances the photocurrent generation efficiency (Figure 7A). IPCE contribution from the CdSe absorption peak at 530 nm increases from 3.8% in CdSe only films to 13.8% in CdSe–RGO composites. CdSe loadings were kept constant in all of these films. The observed enhancement in the IPCE is attributed to the indirect participation of RGO in accepting electrons and shuttling them to the collecting electrode surface. The photocurrent enhancement observed in RGO–CdSe composites has also been shown in CdS and TiO_2 composites with C_{60} and carbon nanotubes.[35,36]

In the present study, preparation of CdSe–(R)GO films by EPD technique allows for increased stacking of quantum dots. When excited with visible light, the charge separation occurs throughout the stack of CdSe particles. However, not all charges can be collected for photocurrent generation. In the absence of RGO, photogenerated electrons in CdSe QD layers farthest from the TiO_2 network are likely to undergo recombination before reaching the collecting electrode surface. The loss of these electrons is evidenced by the low IPCE values of CdSe-only films at 530 nm. Thus, the charge recombination at the grain boundaries limits the overall collection efficiency at the collecting electrode. Collection of photogenerated electrons through the RGO network in CdSe–(R)GO composite films is expected to minimize charge recombination losses. The higher IPCE values obtained with RGO further ascertain its important role in interacting with the excited CdSe and facilitating electron transport within the film. Future work aimed at optimizing current collection in CdSe–RGO composites could incorporate the use of solvent-exfoliated graphene, which is free from the oxidation/reduction-induced defects found in (R)GO. Fewer defects, in turn, would potentially result in improved electron transfer and current collection.[37,38]

Figure 7B shows the photocurrent–time profiles during on–off cycles of illumination. The observed higher current in CdSe-RGO films follows the trend observed in the IPCE spectra. During the first cycle of illumination, we observe a slow rise in the photocurrent of CdSe-GO films. This rise in photocurrent reflects the reduction of GO within CdSe–GO composites during the initial illumination period. As discussed in preceding sections, the photogenerated electrons are first consumed in the reduction of GO, thus enabling the recovery of conductivity within graphene sheets. The rise in the photocurrent is much less pronounced during third cycle of illumination. In fact, under extended illumination (t > 30 min), films made from CdSe–GO composites achieve photocurrent levels within ~15% of CdSe–RGO composites.

CONCLUSION

Upon photoexcitation, CdSe QDs undergo electron transfer to GO resulting in reduction and electron storage. Relative rates of electron and energy transfer from CdSe QDs to GO determined by comparing differences in CdSe–GO PL lifetime characteristics before and after prolonged illumination show comparable kinetic profiles. Provided that a high degree of graphene dispersion within a QD film is achieved, it is possible to leverage the atomic thinness, large surface area and conductivity of graphene to extend useful QD loading into the third dimension. The enhanced photoresponse of EPD-created films of highly dispersed graphene–CdSe QD composites demonstrate the beneficial nature of electron

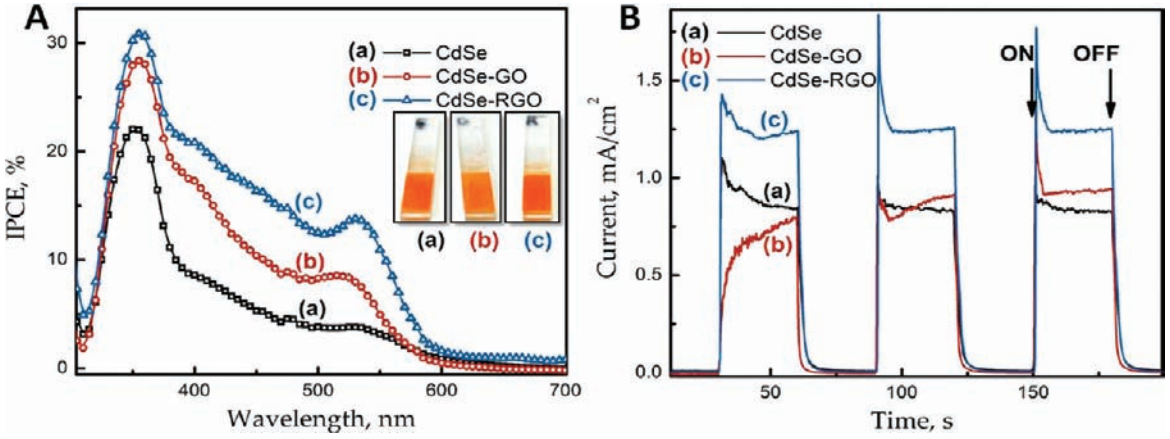

Figure 7. (A) Incident photon to current efficiency (IPCE) of CdSe and CdSe–(R)GO films. Contribution of CdSe QDs (~530 nm) to current generation is markedly improved in CdSe–RGO films. (B) The photocurrent response of CdSe and CdSe–(R)GO composite films to ON-OFF illumination (AM 1.5) cycles. The electrophoretically deposited (a) CdSe, (b) CdSe–GO, and (c) CdSe–RGO films on optically transparent electrodes (OTE) were used as a photoanodes and Cu_2S/RGO as counter electrode with aqueous 0.1 M Na_2S as the electrolyte in each set of experiments.

dx.doi.org/10.1021/ja3012929 | J. Am. Chem. Soc. 2012, 134, 7109–7116

transfer through graphene sheets in QD films. Incorporation of graphene in QD films represents a significant step toward overcoming conductivity problems inherent to QD films, and as such, opens a new avenue toward improved sensitizer loading and performance in QDSCs.

EXPERIMENTAL SECTION

Quantum Dot Synthesis. Quantum dots were synthesized using a modified Peng prep.[39] All materials were purchased from Sigma Aldrich unless otherwise noted. A typical QD preparation involved heating 0.15 g of CdO (99.998%, Alfa Aesar), 2 g of trioctylphosphine oxide (99%, STREM Chemicals), 0.3 g of *n*-tetradecylphosphonic acid (PCI Synthesis) and 1 g of dodecylamine to ∼100 °C for 1 h under vacuum. Mixture was then heated to ∼300 °C and 4.25 mL of 0.0588 M solution of Se (powder, −100 mesh, 99.5%) in trioctylposhpine (90%) was injected. After growth of CdSe QDs to desired color, reaction vessel was cooled and QDs were purified by adding methanol followed by centrifugation (×3). QDs were resuspended in toluene for use.

Graphene Oxide Synthesis. GO was synthesized using a modified Hummers' method and a portion was subsequently reduced solvothermally, described elsewhere.[40−42] Briefly, 200 mg of graphite powder (conducting grade, −325 mesh, 99.9995%, Alfa Aesar), 200 mg of $NaNO_3$, and 9.2 mL of conc. H_2SO_4 were mixed in an ice bath while 1.2 g of $KMnO_4$ was slowly added over a period of ∼30 min. The temperature was then raised to 35 °C and held for 1 h with mixing. Deionized water (10 mL) was added very slowly, taking care solution temperature did not exceed 100 °C. Next, 60 mL of 3% H_2O_2 (Fisher), was added. Finally, the mixture was washed and filtered with HCl (×2), deionized water (×2), and ethanol (×2). GO was suspended in ethanol (0.5 mg/mL) for use. Chemical reduction was avoided to prevent residual hydrazine from convoluting excited state dynamics.

CdSe-Graphene Optical Characterization. GO and RGO dispersions were added to CdSe colloidal quantum dots, with typical graphene concentrations between 18 and 90 μg/mL. Electronic interactions, including excited state dynamics, between colloidal CdSe QDs and dispersed GO and RGO were characterized using UV−vis absorbance spectroscopy (Cary Bio Spectrophotometer), photoluminescence steady state measurements (Jobin Yvon Fluorlog-3), photoluminescence lifetime decay (Jobin Yvon single photon counting system with a 453 nm LED excitation source) and femtosecond transient absorption spectroscopy (Clark MXR-2010 775 nm fundamental laser system described previously[43,44]). Composites were imaged using transmission electron microscopy (TEM). TEM micrographs were taken using FEI Titan 300 kV field emission TEM with Gatan Image Filter. Composite dispersions were formed via simple mixing, no linker or other binding method or material was used to unite the two species.

Photoanode Preparation. TiO_2 films were predeposited via doctor blade method and annealed at 500 °C. CdSe−(R)GO films were created by electrophoretic deposition of CdSe−(R)GO dispersions typically consisting of 50 μL of 9.0 × 10^{-6} M CdSe QDs in toluene and 30 μL of 0.5 mg/mL (R)GO in ethanol, combined in a 0.8:1.0 mixture of toluene/acetonitrile. Briefly, two fluorine-doped tin oxide electrodes were held apart at a constant distance of 4 mm in the EPD dispersion while a potential of 50 V was applied. EPD cycles consisted of 1 min deposition periods followed by remixing.

Photoelectrochemical Testing. Photoelectrochemical testing was carried out using a Princeton Applied Research 2273 (PARstat) potentiostat. A 1 cm cuvette with a Cu_2S−RGO counter electrode and 0.1 M Na_2S electrolyte was used in a two-electrode, open cell configuration. A 300 W Xe lamp with AM 1.5 filter was used to illuminate the active area at 100 mW/cm^2. The photoanode active area was ∼1.6 cm^2. The distance between photoanode and counter electrode was held at ∼7 mm.

ASSOCIATED CONTENT

Supporting Information

Ultrafast transient absorption measurements were conducted to further elucidate electron transfer in CdSe−(R)GO composites. Figure S1 depicts the absorption bleach recovery in CdSe and CdSe−GO composites. The transient absorption kinetic traces for CdSe, CdSe−GO, and CdSe−RGO composites are shown in Figure S2. This material is available free of charge via the Internet at http://pubs.acs.org.

AUTHOR INFORMATION

Corresponding Author

pkamat@nd.edu

Notes

The authors declare no competing financial interest.

ACKNOWLEDGMENTS

The research described herein was supported by the Division of Chemical Sciences, Geosciences, and Biosciences, Office of Basic Energy Sciences of the U.S. Department of Energy through Award DE-FC02-04ER15533. This is contribution number NDRL 4913 from the Notre Dame Radiation Laboratory.

REFERENCES

(1) Norris, D. J.; Bawendi, M. G. *Phys. Rev. B* **1996**, *53*, 16338.
(2) Yu, W. W.; Qu, L. H.; Guo, W. Z.; Peng, X. G. *Chem. Mater.* **2003**, *15*, 2854.
(3) Mews, A.; Eychmuller, A.; Giersig, M.; Schooss, D.; Weller, H. *J. Phys. Chem.* **1994**, *98*, 934.
(4) Vogel, R.; Pohl, K.; Weller, H. *Chem. Phys. Lett.* **1990**, *174*, 241.
(5) Shockley, W.; Queisser, H. J. *J. Appl. Phys.* **1961**, *32*, 510.
(6) Barea, E. M.; Shalom, M.; Giménez, S.; Hod, I.; Mora-Seró, I. n.; Zaban, A.; Bisquert, J. *J. Am. Chem. Soc.* **2010**, *132*, 6834.
(7) Hodes, G.; Cahen, D.; Manassen, J.; David, M. *J. Electrochem. Soc.* **1980**, *127*, 2252.
(8) Gonzalez-Pedro, V.; Xu, X.; Mora-Sero, I.; Bisquert, J. *ACS Nano* **2010**, *4*, 5783.
(9) Deng, M. H.; Huang, S. Q.; Zhang, Q. X.; Li, D. M.; Luo, Y. H.; Shen, Q.; Toyoda, T.; Meng, Q. B. *Chem. Lett.* **2010**, *39*, 1168.
(10) Tachan, Z.; Shalom, M.; Hod, I.; Ruhle, S.; Tirosh, S.; Zaban, A. *J. Phys. Chem. C* **2011**, *115*, 6162.
(11) van de Lagemaat, J.; Frank, A. J. *J. Phys. Chem. B* **2001**, *105*, 11194.
(12) Chandler, R. E.; Houtepen, A. J.; Nelson, J.; Vanmaekelbergh, D. *Phys. Rev. B* **2007**, 75.
(13) Niitsoo, O.; Sarkar, S. K.; Pejoux, C.; Ruhle, S.; Cahen, D.; Hodes, G. *J. Photochem. Photobiol. A, Chem.* **2006**, *181*, 306.
(14) Diguna, L. J.; Shen, Q.; Kobayashi, J.; Toyoda, T. *Appl. Phys. Lett.* **2007**, *91*, Art. No: 023116
(15) Lee, H.; Wang, M. K.; Chen, P.; Gamelin, D. R.; Zakeeruddin, S. M.; Gratzel, M.; Nazeeruddin, M. K. *Nano Lett.* **2009**, *9*, 4221.
(16) Wang, D. W.; Li, F.; Zhao, J. P.; Ren, W. C.; Chen, Z. G.; Tan, J.; Wu, Z. S.; Gentle, I.; Lu, G. Q.; Cheng, H. M. *ACS Nano* **2009**, *3*, 1745.
(17) Eda, G.; Chhowalla, M. *Nano Lett.* **2009**, *9*, 814.
(18) Kamat, P. V. *J. Phys. Chem. Lett.* **2011**, *2*, 242.
(19) Cui, Y.; Wang, H. L.; Cui, L. F.; Yang, Y. A.; Casalongue, H. S.; Robinson, J. T.; Liang, Y. Y.; Dai, H. J. *J. Am. Chem. Soc.* **2010**, *132*, 13978.
(20) Yoo, E.; Kim, J.; Hosono, E.; Zhou, H.-s.; Kudo, T.; Honma, I. *Nano Lett.* **2008**, *8*, 2277.
(21) Seger, B.; Kamat, P. V. *J. Phys. Chem. C* **2009**, *113*, 7990.
(22) Liu, Z.; Robinson, J. T.; Sun, X. M.; Dai, H. J. *J. Am. Chem. Soc.* **2008**, *130*, 10876.
(23) Williams, G.; Seger, B.; Kamat, P. V. *ACS Nano* **2008**, *2*, 1487.

(24) Ng, Y. H.; Lightcap, I. V.; Goodwin, K.; Matsumura, M.; Kamat, P. V. *J. Phys. Chem. Lett.* **2010**, *1*, 2222.
(25) Stankovich, S.; Dikin, D. A.; Dommett, G. H. B.; Kohlhaas, K. M.; Zimney, E. J.; Stach, E. A.; Piner, R. D.; Nguyen, S. T.; Ruoff, R. S. *Nature* **2006**, *442*, 282.
(26) Guo, C. X.; Yang, H. B.; Sheng, Z. M.; Lu, Z. S.; Song, Q. L.; Li, C. M. *Angew. Chem., Int. Ed.* **2010**, *49*, 3014.
(27) Pan, N.; Lin, Y.; Zhang, K.; Chen, W. F.; Liu, Y. D.; Geng, Z. G.; Zeng, J.; Yan, L. F.; Wang, X. P.; Hou, J. G. *ACS Nano* **2010**, *4*, 3033.
(28) Nair, R. R.; Blake, P.; Grigorenko, A. N.; Novoselov, K. S.; Booth, T. J.; Stauber, T.; Peres, N. M. R.; Geim, A. K. *Science* **2008**, *320*, 1308.
(29) Chen, Z. Y.; Berciaud, S.; Nuckolls, C.; Heinz, T. F.; Brus, L. E. *ACS Nano* **2010**, *4*, 2964.
(30) Lightcap, I. V.; Kosel, T. H.; Kamat, P. V. *Nano Lett.* **2010**, *10*, 577.
(31) Yu, D. S.; Park, K.; Durstock, M.; Dai, L. M. *J. Phys. Chem. Lett.* **2011**, *2*, 1113.
(32) Liu, Q.; Liu, Z. F.; Zhong, X. Y.; Yang, L. Y.; Zhang, N.; Pan, G. L.; Yin, S. G.; Chen, Y.; Wei, J. *Adv. Funct. Mater.* **2009**, *19*, 894.
(33) Brown, P.; Kamat, P. V. *J. Am. Chem. Soc.* **2008**, *130*, 8890.
(34) Radich, J. G.; Dwyer, R.; Kamat, P. V. *J. Phys. Chem. Lett.* **2011**, *2*, 2453.
(35) Robel, I.; Bunker, B.; Kamat, P. V. *Adv. Mater.* **2005**, *17*, 2458.
(36) Brown, P.; Kamat, P. V. *J. Am. Chem. Soc.* **2008**, *130*, 8890.
(37) Gomez-Navarro, C.; Meyer, J. C.; Sundaram, R. S.; Chuvilin, A.; Kurasch, S.; Burghard, M.; Kern, K.; Kaiser, U. *Nano Lett.* **2010**, *10*, 1144.
(38) Liang, Y. T.; Vijayan, B. K.; Gray, K. A.; Hersam, M. C. *Nano Lett.* **2011**, *11*, 2865.
(39) Peng, Z. A.; Peng, X. *J. Am. Chem. Soc.* **2001**, *123*, 183.
(40) Hummers, W. S.; Offeman, R. E. *J. Am. Chem. Soc.* **1958**, *80*, 1339.
(41) Abdelsayed, V.; Moussa, S.; Hassan, H. M.; Aluri, H. S.; Collinson, M. M.; El-Shall, M. S. *J. Phys. Chem. Lett.* **2010**, *1*, 2804.
(42) Wang, H. L.; Robinson, J. T.; Li, X. L.; Dai, H. J. *J. Am. Chem. Soc.* **2009**, *131*, 9910.
(43) Robel, I.; Kuno, M.; Kamat, P. V. *J. Am. Chem. Soc.* **2007**, *129*, 4136.
(44) Robel, I.; Subramanian, V.; Kuno, M.; Kamat, P. V. *J. Am. Chem. Soc.* **2006**, *128*, 2385.